Journal of Controlled Release 245 (2017) 70–80

Contents lists available at ScienceDirect

Journal of Controlled Release

journal homepage: www.elsevier.com/locate/jconrel

Sonoporation with Acoustic Cluster Therapy (ACT®) induces transient tumour volume reduction in a subcutaneous xenograft model of pancreatic ductal adenocarcinoma

Spiros Kotopoulis [a,b], Endre Stigen [c,a], Mihaela Popa [d,e], Mireia Mayoral Safont [c], Andrew Healey [f], Svein Kvåle [f], Per Sontum [f], Bjørn Tore Gjertsen [g,h], Odd Helge Gilja [a,b], Emmet McCormack [c,g,h,*]

[a] National Centre for Ultrasound in Gastroenterology, Haukeland University Hospital, Jonas Lies vei 65, 5021 Bergen, Norway
[b] Department of Clinical Medicine, University of Bergen, Jonas Lies vei 65, 5021 Bergen, Norway
[c] Department of Clinical Science, Haukeland University Hospital, Jonas Lies vei 65, 5021 Bergen, Norway
[d] Department of Medicine, Haukeland University Hospital, Jonas Lies vei 65, 5021 Bergen, Norway
[e] KinN Therapeutics AS, Jonas Lies vei 65, 5021 Bergen, Norway
[f] Phoenix Solutions AS, Nycoveien 2, 0485 Oslo, Norway
[g] Department of Internal Medicine, Haematology Section, Haukeland University Hospital, Jonas Lies vei 65, Bergen 5021, Norway
[h] Centre for Cancer Biomarkers CCBIO, Department of Clinical Science, University of Bergen, Bergen 5021, Norway.

ARTICLE INFO

Article history:
Received 5 August 2016
Received in revised form 8 November 2016
Accepted 17 November 2016
Available online 18 November 2016

Keywords:
Sonoporation
Acoustic Cluster Therapy
Pancreatic ductal adenocarcinoma
Mouse model
Ultrasound
Microbubbles

ABSTRACT

Pancreatic ductal adenocarcinoma (PDAC) remains one of the deadliest cancers with survival averaging only 3 months if untreated following diagnosis. A major limitation in effectively treating PDAC using conventional and targeted chemotherapeutic agents, is inadequate drug delivery to the target location, predominantly due to a poorly vascularised, desmoplastic tumour microenvironment. Ultrasound in combination with ultrasound contrast agents, i.e., microbubbles, that flow through the vasculature and capillaries can be used to disrupt such mechanical barriers, potentially allowing for a greater therapeutic efficacy. This phenomenon is commonly referred to as sonoporation. In an attempt to improve the efficacy of sonoporation, novel microbubble formulations are being developed to address the limitation of commercially produced clinical diagnostic ultrasound contrast agents.

In our work here we evaluate the ability of a novel formulation; namely Acoustic Cluster Therapy (ACT®) to improve the therapeutic efficacy of the chemotherapeutic agent paclitaxel, longitudinally in a xenograft model of PDAC. Results indicated that ACT® bubbles alone demonstrated no observable toxic effects, whilst ACT® in combination with paclitaxel can transiently reduce tumour volumes significantly, three days posttreatment ($p = 0.0347–0.0458$). Quantitative 3D ultrasound validated the calliper measurements. Power Doppler ultrasound imaging indicated that ACT® in combination with paclitaxel was able to transiently sustain peak vasculature percentages as observed in the initial stages of tumour development. Nevertheless, there was no significant difference in tumour vasculature percentage at the end of treatment. The high vascular percentage correlated to the transient decrease and overall inhibition of the tumour volumes.

In conclusion, ACT® improves the therapeutic efficacy of paclitaxel in a PDAC xenograft model allowing for transient tumour volume reduction and sustained tumour vasculature percentage.

1. Introduction

Pancreatic ductal adenocarcinoma (PDAC) remains one of the most deadly cancers with survival averaging only 3 months if untreated following diagnosis [1,2]. The current clinical regimes are chemotherapy and/or surgery, with or without radiation therapy. Whilst surgery remains the only potential for cure, it is rarely an option due to its late diagnosis and invasive nature [3]. Even the most effective chemotherapeutic regime (FOLFIRINOX) results in a median overall survival of 26.6 months in patients with locally advanced pancreatic cancer, *i.e.*, no metastasis [4]. If a tumour is downgraded following treatment allowing for the possibility of surgery, overall survival increases to 35.4 months [5] indicating the importance of tumour volume reduction.

A major limitation in effectively treating such solid tumours using therapeutic agents, such as chemotherapeutics, is the inadequate delivery to the target location whether due to tumour interstitial fluid pressure [6], lack of vascularisation or perfusion [7], or the presence of a dense stromal matrix [8,9]. The stromal microenvironment is a complex

* Corresponding author at: Department of Internal Medicine, Haematology Section, Haukeland University Hospital, Jonas Lies vei 65, Bergen 5021, Norway.
E-mail address: Emmet.Mc.Cormack@med.uib.no (E. McCormack).

http://dx.doi.org/10.1016/j.jconrel.2016.11.019
0168-3659/

structure composed of an extracellular matrix (ECM), activated fibroblasts and myofibroblasts, inflammatory cells and blood and lymphatic vessels that distort the normal architecture of pancreatic tissue. The complex interplay between tumour cells and stroma promotes cancer cell motility, resistance to hypoxia and stromal neovascularization [8]. These physical barriers result in inaccessibility to the tumour for most chemotherapeutic agents. As a result, irrespective of how good the targeted approach, all chemotherapeutic treatments suffer the same fate *in vivo*, whilst increasing dosage to compensate only exasperates systemic side effects [10]. Thus, mechanical disruption of the tumour or normalisation of tumour vascularisation to permit enhanced delivery of therapeutics may provide greater clinical promise. Novel therapeutic options specifically targeted at treating solid tumours are currently under investigation, including nanoparticles [11,12], molecular targeting [13,14], and ultrasound- and microbubble-mediated therapy [15–17] *i.e.*, sonoporation.

Sonoporation is a novel methodology where gas microbubbles are injected into the vasculature and excited by ultrasound (US) to invoke biomechanical effects that increase the permeability of the vascular barrier and extravasation of drug in a specific location [18,19]. Microbubbles are stabilized gas bubbles (2–3 μm in diameter) that are injected intravascularly and are typically stable for up to 5 min *in vivo* with no known side-effects. Upon the application of ultrasound, these microbubbles volumetrically oscillate and interact with nearby cells forming small pores in the cell membrane via mechanical disruption and even been observed to enter the cells *in vitro* [20]. This interaction permits increased intracellular drug uptake [21] whilst also allowing therapeutic agents deeper penetration into the tissue than the vascular barrier alone [22]. As a result, sonoporation can improve the therapeutic efficacy of intravascularly injected therapeutic agents.

Previously, we have demonstrated that combining sonoporation with gemcitabine in an orthotopic xenograft model of gemcitabine resistant PDAC could inhibit tumour growth up to four-fold in comparison to gemcitabine monotherapy [16]. A subsequent Phase I clinical trial also indicated that sonoporation has the potential to transiently decrease tumour volume in patients with locally advanced or metastatic pancreatic ductal adenocarcinoma (PDAC) [15,17]. Whilst these studies show promise, the true potential of sonoporation is limited due to the use of commercially available microbubbles designed and optimised for ultrasound imaging, not therapy. As a result, substantial research is focusing on developing "next-generation" microbubbles optimised for ultrasound-target and -enhanced therapy. Specifically, the major limitation has been that currently sonoporation requires the co-administration of the therapeutic agent; resultantly similar systemic side effects are experienced. A secondary limitation is the size of microbubbles. It has been hypothesised that smaller bubbles are required to enter the sub-micron sized fenestrations presented in tumours [23]. However, it has also been suggested that larger bubbles may have a stronger sonoporation effect leading to deeper penetration of the drug and enhanced therapeutic efficacy [24].

To address the current limitations of commercial bubbles for therapy, a range of novel microbubbles are being developed [25–36]. Acoustic Cluster Therapy is a novel concept for ultrasound mediated, targeted drug delivery (ACT®, Phoenix Solutions AS, Oslo, Norway) [37].

ACT® is an ultrasound-activated formulation combining negatively charged, commercially available and clinically employed microbubbles (Sonazoid, GE Healthcare, Little Chalfont, United Kingdom) (Fig. 1-A1) with positively charged microdroplets (Fig. 1-A2). A mixture of these microbubbles and microdroplets results in small microbubble-microdroplets clusters held together by the electrostatic forces (Fig. 1-A3). The microdroplets consist of a fully or partially fluorinated or halogenated oil component (PF-X) that has a boiling temperature of <50 °C, low blood solubility. The ACT® cluster dispersion is intended for co-administration with a drug. A lipophilic therapeutic agent may optionally be embedded into the microdroplets. When these clusters are insonated with ultrasound (in the clinical diagnostic regime) the volumetrically oscillating microbubbles transfer energy to the microdroplet initiating vaporisation [37]. These 20–30 μm ACT® bubbles have been shown to form in capillary sized vessels in vivo [38,39] and can be used to induce sonoporation by exciting them at low frequencies (0.3–1.0 MHz). In addition, if a therapeutic agent is embedded in the oil, it will be released in the activation region resulting in ultrasound guided and targeted release.

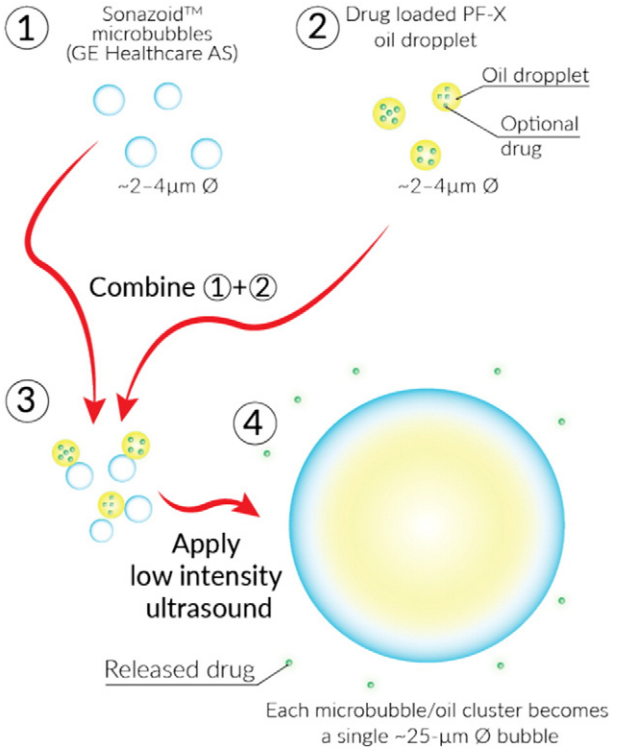

Fig. 1. Graphical representation of the ACT® principle. Sonazoid™ microbubbles are combined with a PF-X oil droplet that can be loaded with a drug. Upon low intensity ultrasound application, the oil droplet vaporises releasing the drug and forming a single large microbubble.

In our work here we evaluate the ability of ACT® to improve the therapeutic efficacy of the chemotherapeutic agent paclitaxel (PTX) in a longitudinal xenograft model of PDAC. We evaluated the therapeutic benefit of ACT® on tumour volume and vasculature over 5 treatment cycles (5 weeks).

2. Materials and methods

Ultra-high-speed imaging was used to visualise the transition from ACT® clusters to single large microbubbles. The ability of ACT® to induce targeted, ultrasound-enhanced chemotherapy therapy was evaluated in a longitudinal study using a subcutaneous xenografted pancreatic cancer murine model. Tumour development was evaluated using 3D B-mode and Power Doppler ultrasound, calliper based tumour volume measurements, and full body bioluminescence imaging. Body weight measurements were performed to evaluate treatment toxicity.

2.1. Ultra-high-speed imaging

Ultra-high-speed imaging of ACT® was performed using a previously described setup. Specifically, the ACT® compound was injected into a 200-μm outer diameter cellulose capillary and imaged through a 60× water immersion objective (NA = 1.0, working distance = 2 mm) (Olympus, Tokyo, Japan). A Kirana ultra-high-speed imaging camera (Specialised Imaging Ltd., Hertfordshire, United Kingdom) was used as the video capture source. A pulsed laser with a 100 ns illumination time was used as the light source and defined the exposure time. Images

were captured at a frame rate of 5 million frames per second, *i.e.*, every 200 ns. A total 180 frames were captured resulting in a video capture time of 36 μs. A 1-MHz,16-mm diameter bowl, with a 16-mm focal distance driven by a 30 cycle burst wave was used as the ultrasound source. The ultrasound transducer was positioned underneath the capillary pointing towards the capillary at an elevation angle of approximately 45°. The acoustic pressure at the height of the capillary was estimated at a peak-negative pressure of 400 kPa, *i.e.*, an MI = 0.4.

The ACT® compound was prepared as per manufacturer's instructions, diluted 10-fold in tap water at room temperature, and injected into the capillary. Experiments were performed with no fluid flow. Fig. 2-A depicts a schematic of the experimental setup and Fig. 2-B shows the correlation of image capture time to the ultrasound excitation cycle.

2.2. Mice

Male NOD-*scid* IL2rγ^{null} mice [40] aged 6–10 weeks old (Vivarium, University of Bergen); originally a generous gift of Prof. Leonard D. Shultz, Jackson Laboratories, Bar Harbor, ME, USA) were used in this experiment. All experiments were approved by The Norwegian Animal Research Authority and conducted according to The European Convention for the Protection of Vertebrates Used for Scientific Purposes, in an AAALAC accredited institution. The 3Rs for animal welfare research were followed in this experiment [41].

2.3. Cell line and cell culture

The human pancreatic adenocarcinoma MIA PaCa-2 cell line [42] (kindly provided by Dr. Anders Movlen, The University of Bergen, Norway) was retrovirally transfected using Phoenix cells [43,44] (LGC Standards AB, Boras, Sweden) and a luciferase-encoding plasmid. High luciferase-expressing cells were selected by puromycin (2.5 μg/ml) [45,46]. These cells grow adherently as single cells and loosely attached clusters. Cells were cultured with Dulbecco's Modified Eagle's Medium-D6429 (DMEM) (Sigma-Aldrich, St. Louis, MO, USA) with 4500 mg/l glucose and 110 mg/l sodium pyruvate. The medium was supplemented with 10% heat-inactivated (56 °C) foetal bovine serum (FBS) (HyClone™ research grade, South-America, Thermo Scientific, Wilmington, DE, USA), 50 UI/ml Penicillin, 50 μg/ml Streptomycin, 2 mM L-glutamine (Sigma-Aldrich, op. cit.) and 2.5% horse serum (HS) (New Zealand, Gibco, Life technologies, MA, USA). The cell line was cultured in 150 mm diameter tissue culture dishes (TPP, Sigma-Aldrich, op. cit.). The cell culture was split 2–3 times a week.

2.4. Test items

Investigated ACT® test items were kindly provided by Phoenix solutions, Oslo, Norway [37]. In brief, the following formulations were investigated;

A) Non-loaded ACT® compound.

Microbubble/microdroplet cluster dispersion comprising Sonazoid™ reconstituted with 2 ml of perfluoromethylcyclopentane (PFMCP) microdroplets (3 μl/ml) stabilized with a distearoylphosphatidylcholine (DSPC) phospholipid membrane with 3% (mol/mol) stearlyamine (SA), dispersed in 5 mM TRIS buffer.

B) Paclitaxel loaded ACT® compound.

Microbubble/microdroplet cluster dispersion comprising Sonazoid™ reconstituted with 2 ml of PFMCP:trichlorofluoropropane:trichloromethane (1:1:1) microdroplets (1.5 μl/ml), containing 67 mg paclitaxel/ml, stabilized with a DSCP membrane with 3% (mol/mol) SA, dispersed in 5 mM TRIS buffer. The paclitaxel concentration in the final cluster dispersion was 100 μg/ml.

2.5. Subcutaneous xenograft model

The MIA PaCa-2^{luc} cells were detached from the culture dishes using 5 mL trypsin-EDTA (Sigma-Aldrich, *op. cit.*), diluted to 250 × 10^6 cells per mL in a solution of PBS:Matrigel (volume ratio 3:1) (BD Biosciences, Franklin Lakes, NJ, USA), and separated into single syringes containing 100-μL (5 × 10^6 cells) solution. A total of 26 mice were subcutaneously injected at the lower dorsal area with a single 100-μL injection of 5 × 10^6 MIA PaCa-2^{luc} cells in a solution to produce a single tumour.

2.6. Tumour development evaluation

2.6.1. Calliper measurements

Calliper measurements were performed every 3–4 days. Once immediately following treatment and three days after treatment. Tumour dimensions were measured using a digital calliper and volume (V) was calculated using the ellipsoid volume formula:

$$V = \frac{\pi\ (l\ \times\ w\ \times\ h)}{6},$$

where *l*, *w*, and *h* are the length, width, and height of tumour respectively. Length was defined as the longest dimension of the tumour. Width

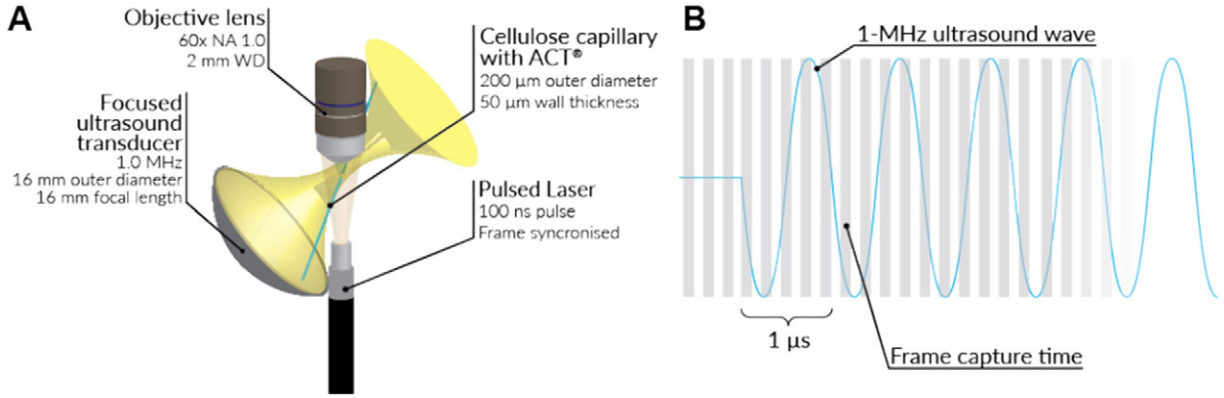

Fig. 2. Graphical representation of experimental setup used to visualise the conversion of ACT® clusters into a single bubble. Panel A shows the arrangement of the experimental configuration. A 1-MHz, 16 mm outer diameter focused ultrasound transducer excited the ACT® clusters that have been injected into the cellulose capillary. A 60×, NA 1.0 objective in combination with a Kirana ultra-high-speed camera is used capture the conversion. Panel B shows the frame time points captured in relation to the 1 MHz ultrasound excitation wave.

was defined as the widest dimension of the tumour perpendicular to the length measurement. The tumour height was measured by slightly lifting the tumour with the skin just enough to fit the calliper measuring tip under the tumour. The maximum height was measured.

2.6.2. Ultrasound imaging

Ultrasound imaging was performed once weekly, prior to treatment. Mice were anaesthetised using isofluorane (Isoba® vet, Intervet, Kenilworth, NJ, USA) in air. Anaesthesia was induced using 3% isofluorane and sustained using 1.5% isofluorane. Anaesthetised mice were placed in a prone position on the heated imaging plate of a Vevo 2100 small animal ultrasound imaging system (Fujifilm VisualSonics Inc., Toronto, Ontario, Canada). Hair on and surrounding the tumour was removed using depilatory cream (Veet™, Reckitt Benckiser, Slough, United Kingdom). Ultrasound imaging was performed using a MS-250 probe. For B-mode imaging, standard general imaging configuration was used with the image size cropped to fit the tumour area. Colour Doppler imaging was used to initially visualise functional vasculature in and around the tumour. A custom power Doppler (PD) configuration with maximum sensitivity and resolution was used. The pulse repetition frequency (PRF) was varied between 1.5 and 2.0 kHz to minimise artefacts. Image width, depth, 3D range, and 3D step size were increased as the tumours grew larger. The display dynamic range was varied between 15 and 20 dB to help delineate the tumour in the B-Mode image. Exact ultrasound imaging settings are shown in Table 1. Three-dimensional B-mode and PD images were captured once a week for all mice until sacrifice. Tumour volume and percentage vasculature were measured in the VEVO software (v1.6.0, VisualSonics Inc., *op. cit.*). Vascular volume was measured using 3D power Doppler imaging. Tumour percentage vascularisation is the percentage of the tumour volume that contained a power Doppler signal.

2.6.3. Optical imaging

Optical imaging was performed once weekly, 3 days after treatment. Mice were anaesthetised using a combination of isofluorane (Isoba® vet, Intervet, Kenilworth, NJ, USA) and oxygen. Anaesthesia was induced using 3% isofluorane and sustained using 1.5% isofluorane. Anaesthetised mice were injected intraperitoneally (IP) with 150-mg/kg D-luciferin [47] (Biosynth AG, Staad, Switzerland) 10 min prior imaging using an In-Vivo FX PRO molecular imaging system (Carestream Health, Inc., Rochester, NY, USA). A white light exposure photograph was initially captured followed by 90 s exposure to capture bioluminescence. Total bioluminescence values were measured using auto ROIs in the Carestream MI software (Standard Edition, v.5.0.6.20, Carestream Health, Inc.).

Table 1
Ultrasound imaging settings from the Vevo 2100 used to image the subcutaneous tumour prior to treatment. Settings that were varied are depicted as a range, *i.e.*, the PRF, depth, width, 3D range, 3D step size, and dynamic range. All other variables were kept constant.

Mode	B-Mode	Power Doppler	Colour Doppler	3D
Transmit				
Frequency (MHz)	16			
Power (%)	100			
PRF (kHz)	1.5 or 2			
Gate	6			
Receive				
Doppler Gain (dB)		35	35	
2D Gain (dB)		18	18	
Depth (mm)		20	15–20	
Width (mm)		23.4	18–23.4	
Beam Angle (degrees)		0	0	
Sensitivity		5	5	
Line Density	Full	Full	Full	
Persistence	Off	Off	High	
ECG/Respiration Gating	Off/On	Off/On	Off/On	
3D Range (mm)				7–28
3D Step Size (μm)				51–70
Display				
Dynamic Range (dB)	15 or 20			
Display Map	G1			
Priority (%)	43–52			

2.7. Treatment groups

Once the tumour volumes reached 50–80 (mm) [3] (calculated from exterior calliper measurements), mice were randomized into 5 groups (groups 1, 2, and 3: $n = 6$ and control groups 4 and 5: $n = 4$) and treated following the routes and schedules described (Table 2). The health status, tumour volume and weight of the mice were monitored twice a week and mice were humanely euthanized when tumour volume reached 1 (cm) [3].

For clearer presentation in the results and discussion section the groups are subsequently called: ACT® + PTX (IP) [Group 1]; PTX loaded ACT® + PTX (IP) [Group 2]; ACT® [Group 3]; PTX [Group 4]; No treatment [Group 5].

The difference between Group 1 and 2 is that in Group 1, 15 mg/kg paclitaxel was injected IP only whilst in Group 2, 0.5 mg/kg paclitaxel was contained in the ACT® microdroplets (injected IV) which was released upon ultrasound activation in addition to the 14.5 mg/kg paclitaxel injected IP. Both Group 1 and Group 2 had a total paclitaxel dose of 15 mg/kg.

2.8. Treatment protocol

Treatment was started on day 14 after inoculation for all groups when the mean tumour volume was 53 ± 3 (mm) [3] when measured by calliper. Mice were randomized into groups with no difference in tumour volume by one-way ANOVA ($p > 0.7$). Treatment was performed once weekly for a total of 5 weeks. The experimental endpoint was defined as when the tumour volume of all mice in the *No treatment* group surpassed 1000 (mm) [3].

Fig. 3 shows the chronological order of ultrasound imaging and treatment for each mouse. Ultrasound imaging was performed prior to treatment and full body bioluminescence was performed three days after treatment allowing the mice to recover from the treatment induced stress.

Mice in Groups 1, 2 and 4 were initially injected IP with 15 mg/kg of Paclitaxel (Fresenius Kabi, 6 mg/ml, batch 21HM0014). After 30 min each mouse was anaesthetised using a combination of isofluorane (Isoba® vet, Intervet, Kenilworth, NJ, USA) and air. Anaesthesia was induced using 3% isofluorane and sustained using 1.5% isofluorane. Oxygen was not used as it changes the extent of blood oxygen window, which is assumed to reduce the microbubble/ACT® temporal stability.

Following ultrasound imaging the mice were removed from the ultrasound-imaging table and transferred to a “treatment station” (Fig. 4).

Table 2
Treatment groups indicating respective treatment, dose, route and number of mice (n). Key: intraperitoneally (IP), intravenously (IV). §Paclitaxel dose in ACT® formulation was 0.5 mg/kg. Total dose of paclitaxel for Group 2 was 15.0 mg/kg.

Group	Treatment	Dose	Route	n
1	Paclitaxel	15.0 mg/kg	IP	6
	ACT® + US	150 nl microdroplets/mouse (50 μl)	IV	
2	Paclitaxel	14.5 mg/kg	IP	6
	Paclitaxel loaded ACT® + US	150 nl microdroplets/mouse (100 μl)§	IV	
3	ACT® + US	150 nl microdroplets/mouse (50 μl)	IV	6
4	Paclitaxel	15 mg/kg	IP	4
5	Control (no treatment)			4

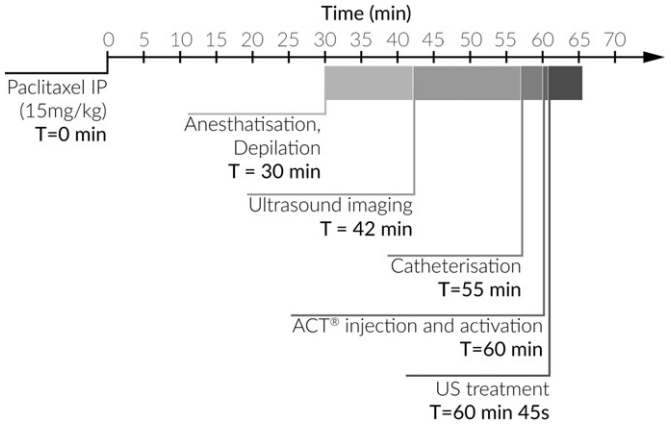

Fig. 3. Chronological diagram depicting initiation and duration of ultrasound imaging and treatment of each mouse. Treatment was started 60 min after paclitaxel injection. ACT® activation lasted 45 s and was followed by 300 kHz ultrasound treatment for 5 min.

Fig. 4 shows photographs of an ACT® test item (*op. cit.*, Section 2.4) being injected IV and activated (Panel A), and treatment using the 300 kHz ultrasound probe (Panel B).

Mice were catheterised in the tail vein using a bespoke catheter consisting of a 30G, 12 mm needle (Omnican, B.Braun, Melsungen AG, Melsungen, Germany) connected to a 15 cm long 0.25 mm inner diameter, chemically inert, hydrophobic Tygon® microbore tube (Part No. VERNAAD04091, VWR International AS, Oslo, Norway). Mice were then placed in prone position on ultrasound absorbing rubber mat (Aptflex F28, Precision Acoustics Ltd., Dorchester, Dorset, United Kingdom) heated to 37 °C. Ultrasound transmission gel (ECO supergel, Ceracarta, Forli, Italy) cover the contact areas between the mouse and ultrasound absorbing mat. Ultrasound transmission gel was spread over the tumour and a Vscan (GE Healthcare, Little Chalfont, United Kingdom) set to B-mode imaging in cardiac mode (Mechanical Index (MI) = 0.8, Thermal Index (TI) = 0.1, imaging depth = 10 cm) was placed gently touching the tumour avoiding any compression. The ACT® test items were subsequently injected via the catheter (duration: 15 s, injection rate: 200 μl/min for group 1 and 3, 400 μl/min for group 2) followed by saline to push all the ACT® test items into the vasculature (duration: 5 s, volume: 0.02 μl, injection rate: 0.5 μl/min). The boundary between the ACT® test items and saline was clearly distinguishable. This allowed for no additional saline to be injected into the vasculature minimising dilution of the ACT® test items. The catheter was immediately removed following completion of injection. The Vscan was kept on the tumour for a total of 45 s. The injection of the ACT® test items took 30 s including the syringe change over.

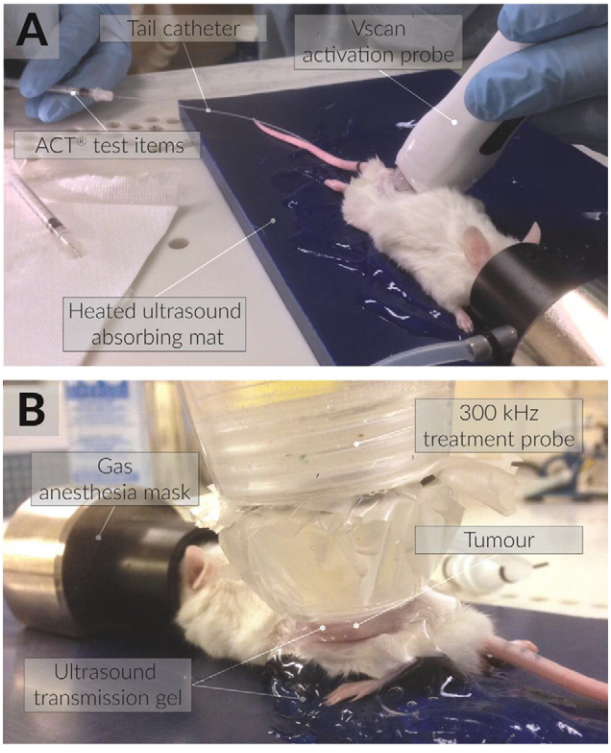

Fig. 4. Photographs of experimental setup. Mouse undergoing ACT® injection and activation (Panel A) and subsequent treatment using the 300-kHz ultrasound probe (Panel B).

Immediately after activation the Vscan was removed and a bespoke computer controlled 300 kHz ultrasound transducer was set in its place to acoustically excite the activated ACT® bubbles with an aim of inducing sonoporation. The 300 kHz ultrasound probe was kept in place for 5 min and acoustic power transmission was monitored via an inbuilt power meter and oscilloscope combined with bespoke software (LabVIEW 2013, National Instruments, Austin, TX, USA) using a continuous closed-loop control.

The acoustic conditions for activation and treatment are shown in Table 3. These acoustic conditions were characterised using an in-house 3-axis calibration system consisting of calibrated needle hydrophones (Precision Acoustics, Ltd., *op. cit.*) in the near field where the tumour would be positioned during ACT® test item activation and treatment. Acoustic attenuation was neglected due to the minimal penetration depth. Fig. S1 shows the acoustic pulses and corresponding frequency spectra. Fig. S2 shows the peak-to-peak pressure field scans including −3 dB and −6 dB contours, and the construction of the bespoke 300 kHz ultrasound transducer.

Treatment was performed on a heated table and with a heat lamp to prevent hypothermia. Mouse body surface temperature was measured using an infrared temperature gauge (Art. No.: 36-5737, Clas Ohlson, Oslo, Norway) and sustained at temperatures equivalent to awake mice (~30–32 °C) [48].

ACT® test items were prepared following manufacturer's instructions. Specifically, the PFMCP vial was homogenized for 30 s by firmly agitating by hand. The rubber stopper of both the PFMCP and Sonazoid™ microbubbles was perforated for venting purposes using a 19G needle, 2.54 cm long needle (B·Braun, *op. cit.*). Immediately after, 2 ml of the PFMCP emulsion was gently withdrawn (duration: 5 s) and injected (duration: 5 s) into the Sonazoid™ vial. Both needles were immediately removed and without delay the final product was homogenized by holding the vial between the thumb and index finger, and gently flipping it 180° back and forth approximately twice a second for 20 s. The preparation procedure took 90–100 s.

The Paclitaxel loaded ACT® test items were prepared using the same procedure. Due to the formulation of the paclitaxel loaded ACT®, the resultant concentration was half that of non-loaded ACT® test items. Hence, twice the volume of paclitaxel-loaded ACT® was used vs. the non-loaded ACT® formulation (*i.e.*, 100 μl vs. 50 μl) resulting in 150 nl

Table 3
Acoustic conditions for activation and treatment.

	Activation	Treatment
Duration (s)	45	300
Peak Frequency [f_c] (MHz)	1.490	0.300
MI	0.44	0.1
I_{SPTA} (mW/cm^2)	2.95	2.39
I_{SPPA} (W/cm^2)	7.03	0.094
Bandwidth [−6 dB] (MHz/%)	0.91/61	0.16/53
Duty cycle (%)	0.18	7.28
Pulse duration (μs)	1.00	25
Pulse Repetition (ms/Hz)	38.3/26.1	1.0/100
Total US time (s)	0.08	21.84

microdroplets per treatment. The 100 μl of the paclitaxel loaded ACT clusters contained 500 ng of paclitaxel at a 5 μg/ml concentration.

Following this protocol, mice were sequentially imaged and treated every 15–20 min.

2.9. Statistical analysis

Results are expressed as mean values ± SEM. Comparisons between groups were made using a two-tailed unpaired Student *t*-test and one-way ANOVA. Differences where $p < 0.05$ were considered as statistically significant. Statistics were analysed using GraphPad PRISM® v6.0a (GraphPad Software Inc., La Jolla, CA, USA) software.

3. Results

General results indicate that ACT® alone- without paclitaxel loading or combination treatment with paclitaxel demonstrated no additional toxicity. However, ACT® was found to improve the treatment efficacy of paclitaxel when compared to paclitaxel monotherapy. Nevertheless, paclitaxel loaded ACT® did not show any improvement versus unloaded ACT®.

3.1. Ultra-high-speed imaging

Ultra-high-speed imaging was used to visualise the conversion from ACT® clusters into a single bubble. An example of this conversion is shown in Fig. 5 and Video 1. Frame $T = 0$ indicates the time prior to ultrasound arrival. Here, an ACT® cluster consisting of two Sonazoid™ microbubbles (black arrows), and one PF-X droplet (white arrows) can be seen. After 2 cycles of ultrasound (+2.00 μs) the Sonazoid™ bubbles show large volumetric oscillations resulting in a blurred image. After four cycles of ultrasound (+4.20 μs) the PF-X oil starts to vaporise. The PF-X vapor enters the two coalesced Sonazoid™ bubbles in <400 ns (from T = +4.20 μs T = +4.60 μs). Volumetric oscillations continue as long as ultrasound is present. At the end of the video recording and ultrasound excitation the cluster has formed a single 6 μm diameter microbubble that continues to grow. After 30 s, (following saving of the video recording) a single large microbubble (circa 20–30 μm in

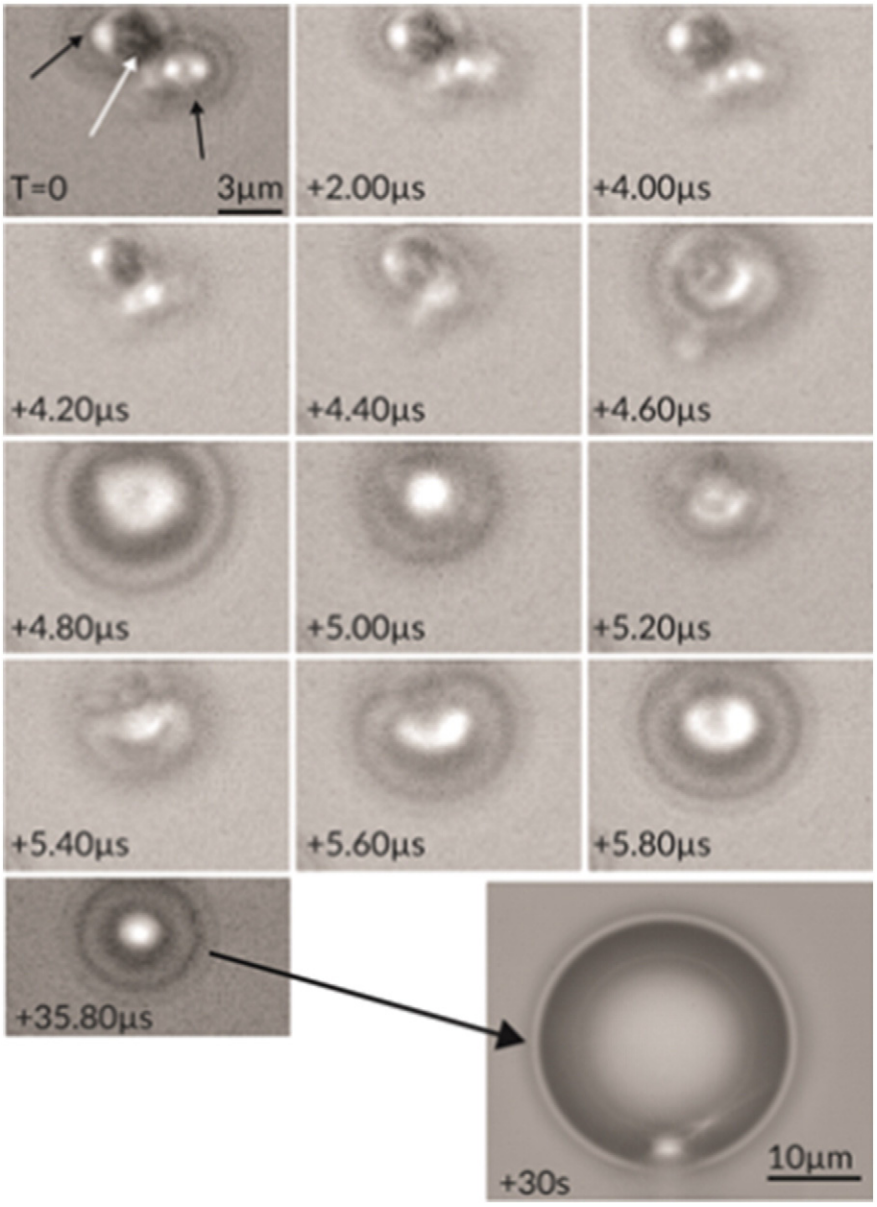

Fig. 5. Ultra-high-speed micrograph showing the conversion of ACT® clusters into a single bubble when excited by 1-MHz ultrasound. In the first panel ($T = 0$) The black arrows are Sonazoid™ microbubbles and the light arrow is a PF-X droplet. Conversion is complete after 5.80 μs. The bubble continues to grow and forms a large 25 μm diameter bubble after 30 s.

diameter, c.f., +30 s Fig. 5) is formed following inward diffusion of gasses in the surrounding liquid.

3.2. Longitudinal toxicity of ACT therapy

Toxicity of this treatment was correlated to measured bodyweight and cage side observations of health, as defined by institutional guidelines. A decrease in body weight of 10% or more from start date was considered to be toxic. Following treatment once weekly over a five-week period, a minor loss in bodyweight was observed in all groups treated with paclitaxel. No decrease in body weight was observed in the group treated with ACT® alone. The decrease in body weight can be attributed to the chemotherapeutic and stress due to anaesthesia, and imaging. The mice always recovered to normal bodyweight on non-dosing days. Throughout the experiments the mice did not exhibit any consistent weight loss surpassing the 10% margin, indicating this treatment has little toxicity. Fig. S3 shows the mean body weight change (%) of each group (±SEM) normalised to pre-treatment weight, as a function of time.

3.3. Therapeutic efficacy of ACT® and paclitaxel in a xenograft model of PDAC

ACT® in combination with paclitaxel was shown to have an effect on tumour volume. Specifically, the groups treated with ACT® in combination with paclitaxel showed inhibited tumour growth.

3.3.1. Calliper measurements

Tumour calliper measurements were performed every 3–4 days. Treatment was initiated on day 14 when tumour volumes had reached

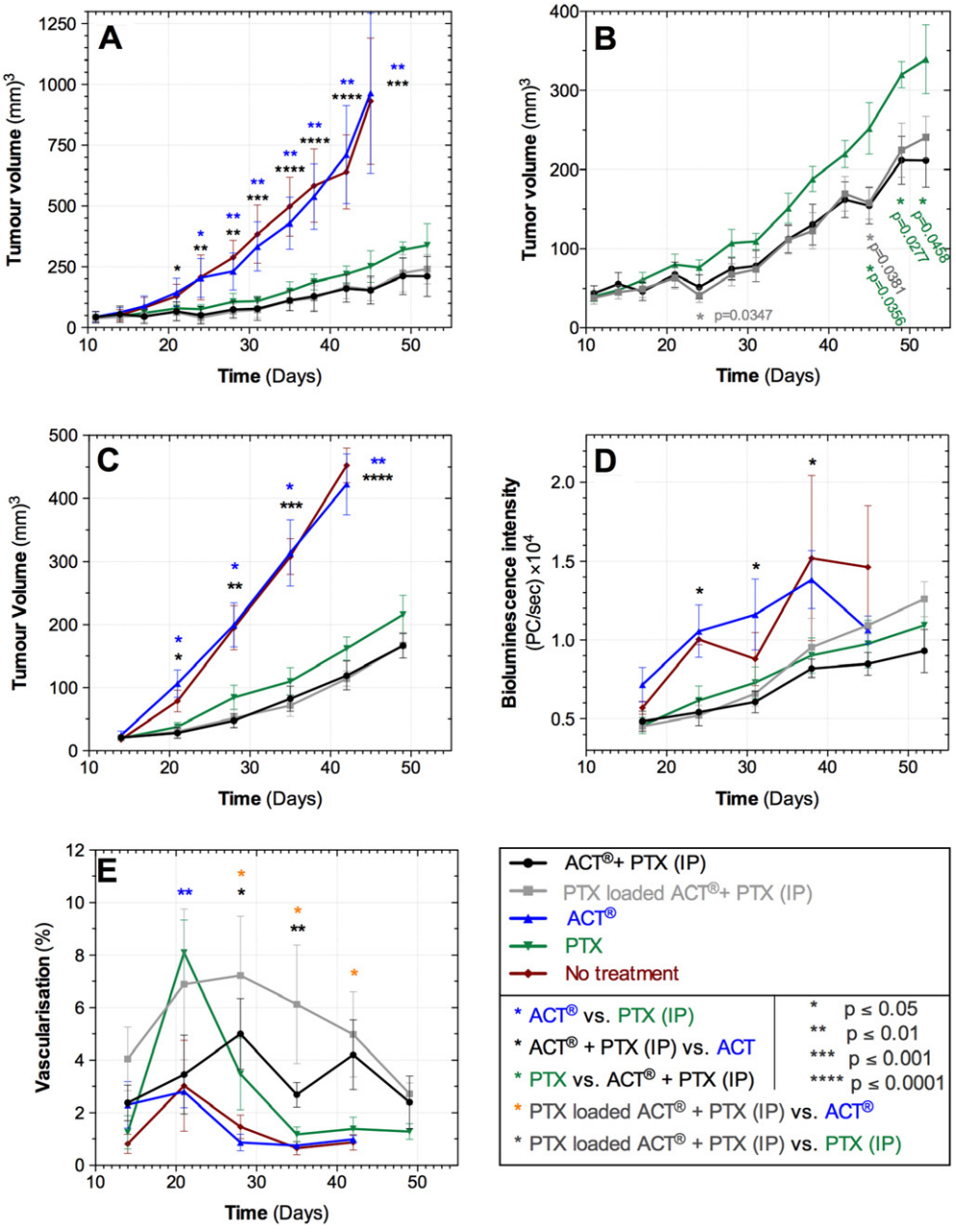

Fig. 6. Quantitative development of tumour as a function of time. Panel A shows the tumour volume of all groups (measured using a vernier calliper) as a function of time. Panel B shows the tumour volume (measured using a vernier calliper) for the three groups treated with paclitaxel as a function of time. Panel C shows the tumour volume of all groups measured using 3D ultrasound as a function of time. Panel D shows the full body bioluminescence intensity for all groups as a function of time. Panel E shows the percentage vasculaturisation measured using power Doppler as a function of time. The stars (*) indicate statistical significance between groups using a student *t*-test.

average volumes 53 (mm) [3], and continued weekly for 5 cycles, as defined in materials and methods. On day 21 a significant difference in tumour volume was observed comparing the groups treated with and without paclitaxel ($0.0257 \leq p \leq 0.0333$) (Fig. 6-A & Table S1). The statistical significance in tumour volume increased with treatment, peaking after 4 treatments (minimum $p < 0.0001$ at 42 days). On day 24 the tumour volume of the group PTX loaded ACT® + PTX (IP) was significantly smaller than the PTX group (PTX = 153 ± 28 (mm) [3] vs. PTX loaded ACT® + PTX (IP) = 108 ± 20 (mm) [3], $p = 0.0347$) (Fig. 6-B). The mean tumour volume of the PTX group decreased 4% from before to after the second treatment, whereas the groups treated with ACT showed a decrease of 34% and 24% for the ACT® + PTX (IP) and PTX loaded ACT® + PTX (IP) groups respectively.

Following the fifth treatment (day 42) both groups (ACT® + PTX (IP) and PTX loaded ACT® + PTX (IP)) showed a significant difference in tumour volume compared to the PTX group ($p = 0.0358$ and 0.0381 respectively). This corresponding to a transient reduction in tumour volume of 5% for the ACT® + PTX (IP) group and 7% for the PTX loaded ACT® + PTX (IP) when comparing before and after the 5th treatment volumes. In contrast the PTX treated group showed an increase of 15% in mean tumour volume. On day 49 and 52 the tumour volumes of the ACT® + PTX (IP) group remained significantly smaller than the PTX group.

Throughout treatment no significant difference in tumour volume observed between the ACT® + PTX (IP) and PTX loaded ACT® + PTX groups.

No difference in tumour volume was observed when comparing ACT® treatment alone to no treatment indicating that ACT® itself had no therapeutic effect (Fig. 6-A).

3.3.2. 3D ultrasound imaging

Results from the 3D ultrasound measurements showed a similar trend to the calliper measurements (Fig. 6-C) where ACT® alone had no effect on the tumour volume, paclitaxel inhibited tumour growth which was enhanced when combined with ACT® or PTX loaded ACT®.

Following a single treatment, the groups treated with paclitaxel had a significantly smaller tumour volume ($p = 0.0058$–0.0318) (Table S1). This difference in tumour volume increased after each treatment cycle. Comparing the tumour volumes for the paclitaxel treated groups the mean tumour volume of the ACT® treated mice was consistently smaller than the PTX group. Nevertheless, the difference was not statistically significant.

Fig. 7 shows a qualitative visualisation of representative tumours from each group as a function of time using 3D ultrasound and manual segmentation. The ACT® + PTX (IP) and PTX loaded ACT® + PTX (IP) groups showed the slowest tumour progression.

3.3.3. Full body bioluminescence

Full body bioluminescence imaging results initially matched the volumetric ultrasound and calliper measurements but with a range within each group (Fig. 6-D). The first measurement was performed three days after treatment (day 17), hence from the first measurement a difference in photon count is observed.

After two treatments the groups treated with PTX showed significantly less bioluminescence than the groups not treated with PTX ($p = 0.0005$–0.0172) (Table S1). Significance was only sustained between the ACT® + PTX (IP) vs. ACT groups following treatment.

Bioluminescence images matched the results observed by the ultrasound measurements. Fig. 8 shows full body bioluminescence images of representative mice. The groups treated with ACT® + PTX and PTX loaded ACT® had the lowest intensities. By day 45 the mice treated with paclitaxel showed bioluminescence intensities similar to those of the untreated mice on day 24 (Fig. 6-D).

3.4. Tumour vascularisation

In all groups maximum tumour vascularisation percentage was observed when tumour volumes were <120 (mm) [3] (c.f., Fig. 6-C vs. -E). Prior to treatment, no significant difference in tumour vascularisation percentage or volume was observed. By day 21, tumour vascularisation percentage increased in all groups, where the PTX group had the mean highest vasculature percentage indicating that paclitaxel has an effect on the tumour vasculature. The following week, (day 28), after two treatments, the PTX, ACT®, and No treatment groups showed a decrease in tumour vasculature percentage. In contrast the groups treated with ACT® + PTX (PTX loaded ACT® + PTX (IP), and ACT® + PTX (IP)) both showed an increase in tumour vasculature percentage. This difference was significant when comparing the ACT® + PTX groups to the ACT group ($p = 0.0237$ and 0.0238) (Table S1). On day 35 the tumour vascularisation declined for all groups yet the significance in tumour vasculature percentage of the ACT® treated groups was

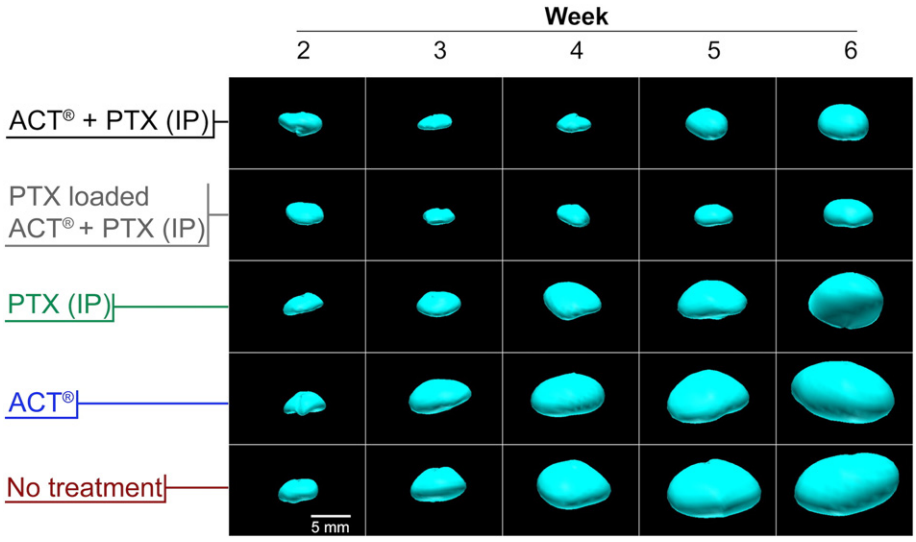

Fig. 7. Volumetric renderings of primary tumour volume in representative mice from each group. A qualitative difference in tumour volume can be observed between mice treated with and without paclitaxel and with and without ACT. ACT alone indicates negligible effect on tumour volume.

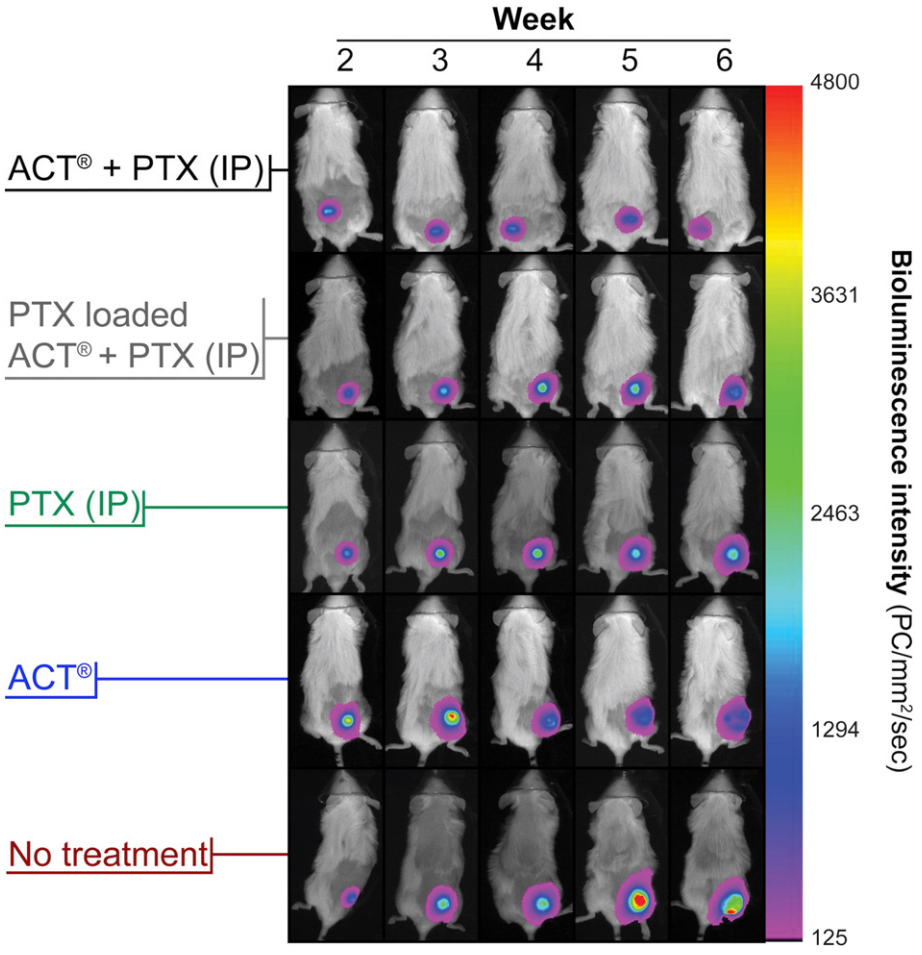

Fig. 8. Optical bioluminescence imaging of MIA PaCa-2^{luc} cells in representative mice treated with combinations of ACT and paclitaxel. The group treated with ACT in combination with paclitaxel had the lowest bioluminescence signal.

sustained or increased. In addition, the tumour percentage vasculature for the PTX loaded ACT® + PTX (IP) group was significantly higher than the PTX group ($p = 0.0424$, PTX loaded ACT® + PTX (IP) = $6.13 \pm 2.26\%$ vs. PTX = $1.17 \pm 0.28\%$). Fig. 9 shows a single slice of maximum vasculature in representative tumours on day 35. Vasculature is depicted by colour Doppler (red and blue). Comparing the mice treated with ACT® + PTX (IP) and PTX loaded ACT® + PTX (IP) to the other groups a distinct difference is observed (Fig. 6-E). The ACT® + PTX mice have large vessels that intersect through the middle of the tumour whilst the other groups only show minor vasculature in the periphery of the tumour.

4. Discussion

Ultra-high-speed imaging showed that the conversion of ACT® clusters into single bubbles required only 5 μs of 1-MHz ultrasound and the

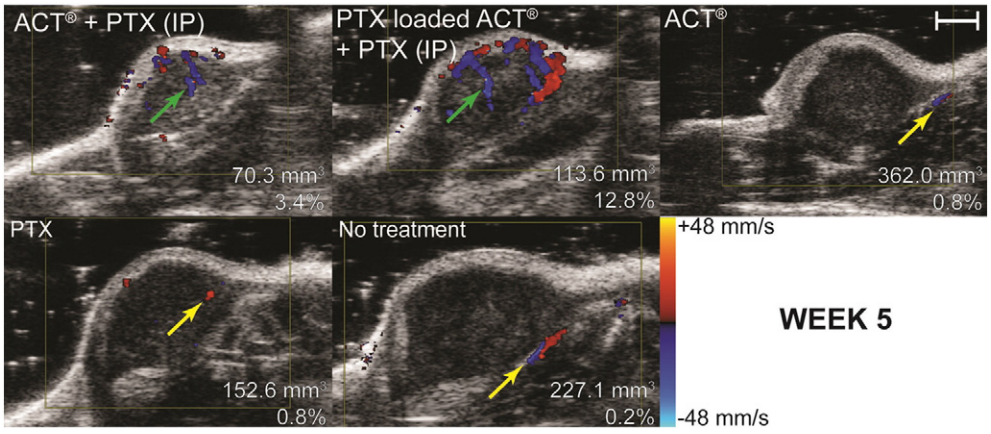

Fig. 9. 2D ultrasound slices through representative tumours at week 5 (day 35) depicting tumour vasculature in red and blue captured using colour Doppler. Green arrows indicated vasculature intersecting the middle of the tumour. Yellow arrows indicate vasculature in the periphery of the tumour. Scale bar indicates 2 mm.

vaporisation of the PF-X oil occurred in less and 1 μs. These results indicate that an activation period of 45 s should be more than sufficient to convert the ACT® clusters into single large bubbles in vivo.

In this pre-clinical PDAC mouse model ACT® therapy in combination with paclitaxel improved the therapeutic efficacy when compared to paclitaxel alone. Specifically calliper measurements demonstrated transient reductions in tumour volumes three days following treatment (when comparing to pre-treatment volumes). In the groups treated with ACT® + PTX tumour volumes did not significantly increase from the start of treatment up to day 24 (Fig. 6-B). This was not observed in any other groups (Fig. 6-A). After the 5th and 6th treatment cycles (day 45 and 52) tumour volume was also transiently reduced three days after treatment. This transient reduction in tumour volume was not observed with the ultrasound measurements due to the temporal resolution, *i.e.*, one vs. two to three measurements per week performed with callipers. These transient reductions in tumour volume may be root of the overall inhibited tumour volumes observed in ACT treated groups.

Power Doppler measurements indicated that ACT® in combination with paclitaxel may have an effect on tumour vascularity and possibly tumour angiogenesis as observed with the vascularisation measurements (Fig. 6-E & Fig. 9). Specifically, ACT® in combination with paclitaxel may sustain the vascularisation percentage in PDAC tumours. In these measurements a large standard error is observed due to the intragroup variation.

On day 31, three days after the 3rd treatment, no transient decrease in tumour volume was observed. This correlated with the drop in vascularisation percentage (*c.f.*, Fig. 6-B day 31 and Fig. 6-E day 35). This may indicate that a sustained vasculature is essential for transient tumour volume reduction, and points to a potential mechanism for the therapeutic enhancement observed with ACT® combinations.

Bioluminescence measurements showed low significance when comparing the ACT® groups with control groups due to the high standard error, an expected result due to the large tumour volumes and resultantly poorly vascularised tumour core. Specifically, the bioluminescence reaction requires ATP and O_2. If ATP or O_2 is insufficient, the light output is not representative of the luciferase activity. When the PDAC tumours grow rapidly, a necrotic/hypoxic core is formed. This phenomenon does not interfere with their growth as tumour cells switch from aerobic to an anaerobic metabolism. Hence the cells require minimal O_2 and ATP synthesis is very low. Consequently, bioluminescence emission is reduced and there is no longer a correlation with tumour volume [49]. In this PDAC model this lack in correlation between tumour volume and bioluminescence activity was observed from tumour volumes above 200 (mm) [3] as measured by 3D ultrasound. Throughout this study, the mice treated with paclitaxel sustained 3D ultrasound measured tumour volumes below 200 (mm) [3]. For these groups, the bioluminescence intensity showed a similar trend to the ultrasound and calliper measurements, albeit with a larger intragroup variation.

Whilst ACT® in combination with paclitaxel has been previously shown to significantly inhibit tumour growth in a prostate cancer model [50], in our work here we evaluate the efficacy of ACT® on a PDAC model. Our cell line used here (MIA PaCa-2) is 8 times more resistant to paclitaxel than the PC-3 cell line [51] used in the previous study, yet the addition of ACT® still resulted in increased tumour growth inhibition. The PDAC tumour model also exhibits significantly lower perfusion and vascularisation [52,53] making it a far more challenging model to treat. We also evaluated the effect of ACT® on the vasculature and correlated it to treatment efficacy. It has been previously shown that inhibiting Hedgehog signalling pathway resulted in depleted tumour associate stromal tissue and increased intra-tumour vascular density leading to disease stabilisation [54,55]. Other studies have demonstrated that by increasing the tumour vasculature in a PDAC model allowed for increased intra-tumour drug delivery which inhibits tumour growth [56]. Our results show a similar response to such studies, where the addition of ACT® to the chemotherapeutic regimen increased/sustained a high vascular density compared to the non-ACT® groups which lead to enhanced tumour growth inhibition. Angiogenesis inhibitors alone, such as PTX have previously shown to have no effect on the late stage vascularity of PDAC tumours [57]. Hence, the increased vascularity observed here may be a result of ACT® treatment in combination with the chemotherapeutic agent inhibiting tumour growth, allowing the vascular network to grow or be sustained, leading to increased therapeutic agent delivery and further enhanced therapy.

A limitation in this study was the low concentration of drug within the PF-X oil. Improving the formulation for higher concentrations may improve the efficacy. In addition, optimising the acoustic treatment conditions (i.e., centre frequency, bandwidth, MI, pulse repetition frequency, and duty cycle) may significantly improve the treatment efficacy. In addition, the transient reduction in tumour volumes suggest that alternate regimes combining lower dose PTX in combination with more frequent, or back-to-back ACT® treatment may render greater therapeutic benefit.

A drawback of ACT® when compared to sonoporation using commercial microbubbles [16,58] the requirement to use two ultrasound frequencies, one to activate, and one to treat. If activation is poor the treatment may be in-effective. Comparing the efficacy of ACT® to previous publications using sonoporation with commercial microbubbles is currently not possible due to the use of a different tumour model (subcutaneous vs. orthotopic) and therapeutic agent (gemcitabine vs. paclitaxel). Nevertheless, in this study, transient tumour volume reduction was observed. As ACT® is still a novel technique and further development on improving the ultrasound emission conditions and the treatment protocol is required. These improvements may improve the efficacy observed in this manuscript.

5. Conclusion

ACT® improves the therapeutic efficacy of paclitaxel in a subcutaneous pancreatic cancer mouse model. ACT® alone was seen to have no effect on tumour development. Three days after treatment a reduction in tumour volume was observed in the ACT® treated groups, whereas chemotherapy alone, only inhibited tumour growth. Groups treated with ACT® in combination with paclitaxel showed a sustained tumour vascularisation percentage when compare to groups treated with paclitaxel or ACT® alone.

Supplementary data to this article can be found online at http://dx.doi.org/10.1016/j.jconrel.2016.11.019.

Acknowledgements

This work was supported by The Research Council of Norway (SonoCURE grant no. 250317), the Norwegian Cancer Society (grant numbers 6833652, 421828 and 732200), the Western Health Board of Norway (grant numbers 911779 and 911182) and the Bergen Research Foundation. The study was supported by MedViz (http://medviz.uib.no/), an interdisciplinary research cluster from Haukeland University Hospital, University of Bergen and Christian Michelsen Research AS. We would like to thank the Molecular Imaging Center (MIC) at the University of Bergen for allowing access to the in vivo imaging systems and Dr. Paul Prentice from the University of Glasgow for access to his ultra-high-speed imaging facilities.

References

[1] M. Malvezzi, P. Bertuccio, F. Levi, C. La Vecchia, E. Negri, European cancer mortality predictions for the year 2014, Ann. Oncol. 25 (2014) 1650–1656.
[2] B.W. Stewart, C.P. Wild, World Cancer Report 2014, World Health Organization, Geneva, 2014 (doi:9283204298).
[3] W. Hartwig, J. Werner, D. Jäger, J. Debus, M.W. Büchler, Improvement of surgical results for pancreatic cancer, Lancet Oncol. 14 (2013) e476–e485.
[4] S.M. Stein, et al., Final analysis of a phase II study of modified FOLFIRINOX in locally advanced and metastatic pancreatic cancer, Br. J. Cancer 114 (2016) 809–812.

[5] M. Khushman, et al., Full dose neoadjuvant FOLFIRINOX is associated with prolonged survival in patients with locally advanced pancreatic adenocarcinoma, Pancreatology 15 (2015) 667–673.
[6] M. Hofmann, et al., Increased plasma colloid osmotic pressure facilitates the uptake of therapeutic macromolecules in a xenograft tumor model, Neoplasia 11 (2009) 812–822.
[7] D.I. Gheonea, C.T. Streba, T. Ciurea, A. Saftoiu, Quantitative low mechanical index contrast-enhanced endoscopic ultrasound for the differential diagnosis of chronic pseudotumoral pancreatitis and pancreatic cancer, BMC Gastroenterol. 13 (2013) 2.
[8] A. Neesse, et al., Stromal biology and therapy in pancreatic cancer, Gut 60 (2011) 861–868.
[9] P.P. Provenzano, S.R. Hingorani, Hyaluronan, fluid pressure, and stromal resistance in pancreas cancer, Br. J. Cancer 108 (2013) 1–8.
[10] G.B. Hans, A. Nakao, J.P. Neoptolemos, S.Y. Peng, M.G. Sarr, Pancreatic Cancer, Cystic Neoplasms and Endocrine Tumors: Diagnosis and Management, Wiley Blackwell, 2015 120–130.
[11] C.R. Patra, R. Bhattacharya, D. Mukhopadhyay, P. Mukherjee, Fabrication of gold nanoparticles for targeted therapy in pancreatic cancer, Adv. Drug Deliv. Rev. 62 (2010) 346–361.
[12] X. Zhao, et al., Co-delivery of HIF1α siRNA and gemcitabine via biocompatible lipid-polymer hybrid nanoparticles for effective treatment of pancreatic cancer, Biomaterials 46 (2015) 13–25.
[13] C. Carbone, D. Melisi, NF-κB as a target for pancreatic cancer therapy, Expert Opin. Ther. Targets 16 (Suppl. 2) (2012) S1–10.
[14] L.A. Chantrill, et al., Precision medicine for advanced pancreas cancer: the individualized molecular pancreatic cancer therapy (IMPaCT) trial, Clin. Cancer Res. 21 (2015) 2029–2037.
[15] S. Kotopoulis, G. Dimcevski, O.H. Gilja, D. Hoem, M. Postema, Treatment of human pancreatic cancer using combined ultrasound, microbubbles, and gemcitabine: a clinical case study, Med. Phys. 40 (2013) 72902.
[16] S. Kotopoulis, et al., Sonoporation-enhanced chemotherapy significantly reduces primary tumour burden in an orthotopic pancreatic cancer xenograft, Mol. Biol. 16 (2014) 53–62.
[17] G. Dimcevski, et al., A human clinical trial using ultrasound and microbubbles to enhance gemcitabine treatment of inoperable pancreatic cancer, J. Control. Release 243 (2016) 172–181.
[18] M. Postema, S. Kotopoulis, A. Delalande, O.H. Gilja, Ultrasound in Gastroenterology. 10-years Anniversary of National Center for Ultrasound in Gastroenterology, 2011 57–59.
[19] M. Postema, S. Kotopoulis, A. Delalande, O.H. Gilja, Sonoporation: why microbubbles create pores, Ultraschall Med. 33 (2012) 97–98.
[20] A. Delalande, S. Kotopoulis, T. Rovers, C. Pichon, M. Postema, Sonoporation at a low mechanical index, Bub. Sci. Eng. Tech. 3 (2011) 3–11.
[21] R.F.J. Kwekkeboom, et al., Increased local delivery of antagomir therapeutics to the rodent myocardium using ultrasound and microbubbles, J. Control. Release 222 (2016) 18–31.
[22] B. Theek, et al., Sonoporation enhances liposome accumulation and penetration in tumors with low EPR, J. Control. Release 231 (2016) 77–85.
[23] T. Inai, et al., Inhibition of vascular endothelial growth factor (VEGF) signaling in cancer causes loss of endothelial fenestrations, regression of tumor vessels, and appearance of basement membrane ghosts, Am. J. Pathol. 165 (2004) 35–52.
[24] Z. Fan, H. Liu, M. Mayer, C.X. Deng, Spatiotemporally controlled single cell sonoporation, Proc. Natl. Acad. Sci. 109 (2012) 16486–16491.
[25] S. Tinkov, R. Bekeredjian, G. Winter, C. Coester, Microbubbles as ultrasound triggered drug carriers, J. Pharm. Sci. 98 (2009) 1935–1961.
[26] S. Tinkov, G. Winter, C. Coester, R. Bekeredjian, New doxorubicin-loaded phospholipid microbubbles for targeted tumor therapy: part I–formulation development and in-vitro characterization, J. Control. Release 143 (2010) 143–150.
[27] R. Abdalkader, et al., Evaluation of the potential of doxorubicin loaded microbubbles as a theranostic modality using a murine tumor model, Acta Biomater. (2015), http://dx.doi.org/10.1016/j.actbio.2015.03.014.
[28] S. Tinkov, et al., New doxorubicin-loaded phospholipid microbubbles for targeted tumor therapy: in-vivo characterization, J. Control. Release 148 (2010) 368–372.
[29] J.S. Xu, et al., Synthesizing and binding dual-mode poly (lactic-co-glycolic acid) (PLGA) nanobubbles for cancer targeting and imaging, Biomaterials 31 (2010) 1716–1722.
[30] C. McEwan, et al., Oxygen carrying microbubbles for enhanced sonodynamic therapy of hypoxic tumours, J. Control. Release 203 (2015) 51–56.
[31] C. McEwan, et al., Combined sonodynamic and antimetabolite therapy for the improved treatment of pancreatic cancer using oxygen loaded microbubbles as a delivery vehicle, Biomaterials 80 (2015) 20–32.
[32] J.A. Kopechek, P. Zhang, M.T. Burgess, T.M. Porter, Synthesis of phase-shift Nanoemulsions with narrow size distributions for acoustic droplet vaporization and bubble-enhanced ultrasound-mediated ablation, J. Vis. Exp. (2012), http://dx.doi.org/10.3791/4308.
[33] P. Zhang, T. Porter, An in vitro study of a phase-shift nanoemulsion: a potential nucleation agent for bubble-enhanced HIFU tumor ablation, Ultrasound Med. Biol. 36 (2010) 1856–1866.
[34] L.C. Phillips, et al., Phase-shift perfluorocarbon agents enhance high intensity focused ultrasound thermal delivery with reduced near-field heating, J. Acoust. Soc. Am. 134 (2013) 1473–1482.
[35] S. Eggen, et al., Ultrasound-enhanced drug delivery in prostate cancer xenografts by nanoparticles stabilizing microbubbles, J. Control. Release 187 (2014) 39–49.
[36] A.K.O. Åslund, et al., Nanoparticle delivery to the brain - by focused ultrasound and self-assembled nanoparticle-stabilized microbubbles, J. Control. Release 220 (2015) 287–294.
[37] P. Sontum, et al., Acoustic cluster therapy (ACT)–a novel concept for ultrasound mediated, targeted drug delivery, Int. J. Pharm. 495 (2015) 1019–1027.
[38] A.v. Wamel, et al., Acoustic cluster therapy (ACT) — pre-clinical proof of principle for local drug delivery and enhanced uptake, J. Control. Release 224 (2016) 158–164.
[39] P. Sontum, et al., Acoustic cluster therapy (ACT) – a novel concept for ultrasound mediated, targeted drug delivery, Int. J. Pharm. 495 (2015) 1019–1027.
[40] L.D. Shultz, et al., Human lymphoid and myeloid cell development in NOD/LtSz-scid IL2R null mice engrafted with mobilized human Hemopoietic stem cells, J. Immunol. 174 (2005) 6477–6489.
[41] D.J. Wells, Animal welfare and the 3Rs in European biomedical research, Ann. N. Y. Acad. Sci. 1245 (2011) 14–16.
[42] Sipos, B. et al. A comprehensive characterization of pancreatic ductal carcinoma cell lines: towards the establishment of an in vitro research platform. Virchows Arch. 442, 444–452
[43] J.B. Lorens, Y. Jang, A.B. Rossi, D.G. Payan, J.M. Bogenberger, Optimization of regulated LTR-mediated expression, Virology 272 (2000) 7–15.
[44] E. McCormack, et al., Synergistic induction of p53 mediated apoptosis by valproic acid and nutlin-3 in acute myeloid leukemia, Leukemia 26 (2012) 910–917.
[45] J. Huang, B.D. Manning, The TSC1-TSC2 complex: a molecular switchboard controlling cell growth, Biochem. J. 412 (2008) 179–190.
[46] A. Baldwin, et al., Kinase requirements in human cells: V. Synthetic lethal interactions between p53 and the protein kinases SGK2 and PAK3, Proc. Natl. Acad. Sci. U. S. A. 107 (2010) 12463–12468.
[47] M. Keyaerts, et al., Dynamic bioluminescence imaging for quantitative tumour burden assessment using IV or IP administration of d-luciferin: effect on intensity, time kinetics and repeatability of photon emission, Eur. J. Nucl. Med. Mol. Imaging 35 (2008) 999–1007.
[48] Y. Saegusa, H. Tabata, Usefulness of infrared thermometry in determining body temperature in mice, J. Vet. Med. Sci. 65 (2003) 1365–1367.
[49] S. Lerondel, A. Le Pape, Bioluminescence imaging in rodents: when light illuminates cancer research, Curr. Mol. Imaging 2 (2013) 18–29.
[50] A. van Wamel, et al., Acoustic cluster therapy (ACT) enhances the therapeutic efficacy of paclitaxel and Abraxane® for treatment of human prostate adenocarcinoma in mice, J. Control. Release 236 (2016) 15–21.
[51] B. Singh, et al., Saccharonol B, a new cytotoxic methylated isocoumarin from Saccharomonospora azurea, Tetrahedron Lett. 54 (2013).
[52] H.J. Lee, et al., Evaluation of tumor angiogenesis in a mouse PC-3 prostate cancer model using dynamic contrast-enhanced sonography, J. Ultrasound Med. 31 (2012) 1223–1231.
[53] G. Korpanty, J.G. Carbon, P.A. Grayburn, J.B. Fleming, R.A. Brekken, Monitoring response to anticancer therapy by targeting microbubbles to tumor vasculature, Clin. Cancer Res. 13 (2007) 323–330.
[54] K.P. Olive, et al., Inhibition of hedgehog signaling enhances delivery of chemotherapy in a mouse model of pancreatic cancer, Science 324 (2009) 1457–1461.
[55] E. Mathew, et al., Dosage-dependent regulation of pancreatic cancer growth and angiogenesis by hedgehog signaling, Cell Rep. 9 (2014).
[56] M.A. Jacobetz, et al., Hyaluronan impairs vascular function and drug delivery in a mouse model of pancreatic cancer, Gut 62 (2013) 112–120.
[57] G. Bergers, D. Hanahan, Modes of resistance to anti-angiogenic therapy, Nat. Rev. Cancer 8 (2008) 592–603.
[58] A. Delalande, et al., Ultrasound and microbubble-assisted gene delivery in Achilles tendons: long lasting gene expression and restoration of fibromodulin KO phenotype, J. Control. Release 156 (2011) 223–230.